In Vivo Targeting of Intratumor Regulatory T Cells Using PEG-Modified Single-Walled Carbon Nanotubes

Cristiano Sacchetti,[†,‡] Novella Rapini,[‡] Andrea Magrini,[§] Elisa Cirelli,[†,∥] Stefano Bellucci,[⊥] Maurizio Mattei,[∥] Nicola Rosato,[#] Nunzio Bottini,*[‡] and Massimo Bottini*[†,#,⊥]

[†]Inflammatory and Infectious Disease Center, Sanford Burnham Medical Research Institute, 10901 North Torrey Pines Road, La Jolla, California 92037, United States

[‡]Division of Cellular Biology, La Jolla Institute for Allergy and Immunology, 9420 Athena Circle, La Jolla, California 92037, United States

[§]Department of Biopathology and Imaging Diagnostics, [∥]Centre for Interdepartmental Services and Animal Technology, [#]Department of Experimental Medicine and Surgery, University of Rome Tor Vergata, Via Montpellier 1, 00133 Rome, Italy

[⊥]INFN, National Laboratory of Frascati, Via Enrico Fermi 40, 00044 Frascati, Rome, Italy

S *Supporting Information*

ABSTRACT: Recent evidence regarding the role of regulatory T cells (T_{reg}) in tumor development has suggested that the manipulation of T_{reg} function selectively in the tumor microenvironment would be a desirable immunotherapy approach. Targeting intratumor immune populations would reduce side effects on peripheral healthy cells and increase antitumor efficacy of immunotherapies. However, no current approaches are available which enable selective *in vivo* targeting of intratumor T_{reg} or other immune cell subpopulations. Herein, we investigated the ability of ligands against T_{reg}-specific receptors to drive selective internalization of PEG-modified single-walled carbon nanotubes (PEG-SWCNTs) into T_{reg} residing in the tumor microenvironment. We focused our attention on the glucocorticoid-induced TNFR-related receptor (GITR), as it showed higher overexpression on intratumor vs peripheral (i.e., splenic) T_{reg} compared to other reported T_{reg}-specific markers (folate receptor 4, CD103, and CD39). *Ex vivo* investigations showed that the T_{reg} targeting efficiency and selectivity of PEG-SWCNTs depended on incubation time, dose, number of ligands per nanotube, and targeted surface marker. *In vivo* investigations showed that PEG-SWCNTs armed with GITR ligands targeted T_{reg} residing in a B16 melanoma more efficiently then intratumor non-T_{reg} or splenic T_{reg}. The latter result was achieved by exploiting a combination of passive tumor targeting due to enhanced tumor vascular permeability, naturally increased intratumor T_{reg} vs effector T cell (T_{eff}) ratio, and active targeting of markers that are enriched in intratumor vs splenic T_{reg}. We also found that PEG-SWCNTs loaded with GITR ligands were internalized by T_{reg} through receptor-mediated endocytosis and transported into the cytoplasm and nucleus *ex vivo* and *in vivo*. This is the first example of intratumor immune cell targeting and we hope it will pave the way to innovative immunotherapies against cancer.
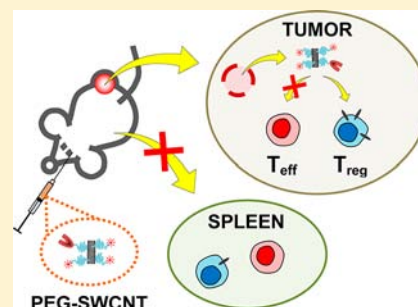
Among T cell subpopulations, $CD4^+CD25^{high}FoxP3^+$ regulatory T cells (T_{reg}), which are able to suppress the response of $CD4^+FoxP3^-$ effector T cells (T_{eff}), have been the object of intense investigation for tumor immunotherapy in the past decade.[1,2] T_{reg} are harnessed by tumors to protect themselves from host antitumor responses. Earlier studies have shown that T_{reg} are present in increased numbers and display an activated phenotype in several tumor microenvironments.[3,4] The increased T_{reg} vs T_{eff} ratio (for example, see Figure S1A) might help shape the tumor microenvironment to enable tumor permissiveness and has provided a rationale for considering systemic T_{reg} depletion an efficient therapeutic approach. However, recent clinical studies have shown that systemic depletion of human T_{reg} is often transient due to quick peripheral T_{reg} replenishment by conversion of T_{eff} into T_{reg}.[5] Furthermore, studies carried out in colon and head and neck cancers suggested that not all intratumor T_{reg} display an

antitumor phenotype and the inflammatory vs noninflammatory nature of the tissue in which the tumor develops determines whether T_{reg} will inhibit or promote tumor development, respectively.[6,7] These observations might help explain why attempts at boosting the antitumor immune response by systemic depletion of T_{reg} have met limited clinical success and suggest that manipulation of T_{reg} function—rather than their systemic depletion—selectively in the tumor microenvironment might be the next frontier of tumor immunotherapy.[8,9] Targeting intratumor immune populations would also reduce side effects on peripheral healthy cells and increase antitumor efficacy of immunotherapies. However, no

current approaches are available that enable efficient and selective *in vivo* targeting of intratumor T_{reg}.

The use of nanodrugs, obtained by loading known drugs into/onto nanotechnology-derived particles (nanoparticles), offers the opportunity to improve the therapeutic index of drugs by altering bioavailability and reducing the potential of side-effects.[10−13] Among the recently developed nanoparticles, PEG-modified single-walled carbon nanotubes (PEG-SWCNTs) have garnered considerable attention in the biomedical community.[14] Because of the PEG-SWCNTs' unique intrinsic properties[15−17] and favorable biological performance,[18−20] several research groups have been investigating PEG-SWCNTs as carriers for targeted delivery of drugs into specific tissues and/or cell subpopulations.[21] Of note, PEG-SWCNTs conjugated to tumor surface marker ligands have been successfully exploited to deliver anticancer drugs into tumor cells due to the excellent permeability and retention (EPR) features of PEG-SWCNTs.[22−27]

Here, we provide proof of principle evidence of efficient and selective targeting of PEG-SWCNTs to intratumor T_{reg} by taking advantage of tumor tissue passive targeting, naturally increased intratumor T_{reg} vs T_{eff} ratio, and active targeting of markers that are enriched on intratumor vs peripheral T_{reg} (Figure 1). We followed a multistep approach: the expression of known T_{reg}-enriched markers was assessed on cell

Figure 1. Intratumor T_{reg}-specific targeting by PEG-SWCNTs. Intratumor CD4+CD25^high^FoxP3+ regulatory T cells [T_{reg}, blue cells (**1**)] were targeted more efficiently and selectively than peripheral (i.e., splenic) T_{reg} by PEG-modified single-walled carbon nanotubes (PEG-SWCNTs) armed with ligands against known T_{reg}-specific receptors (i.e., glucocorticoid-induced TNFR-related receptor). This result was achieved by exploiting a combination of passive targeting due to enhanced tumor vascular permeability (big yellow arrows) and poor lymphatic drainage (not shown), active targeting of markers that are enriched in intratumor vs peripheral T_{reg} (a T_{reg}-specific marker is depicted 3-fold more expressed on intratumor than splenic T_{reg}) and naturally increased intratumor ratio between T_{reg} and other cells subsets [i.e., CD4+FoxP3− "effector" T cell, T_{eff} (**2**)] (T_{reg} vs T_{eff} ratio is depicted 4-fold higher in the tumor than in the spleen). Highly efficient and selective targeting of intratumor T_{reg} is depicted by the big arrow pointing to T_{reg} and the crossed small arrow pointing to other cell subsets [i.e., T_{eff}, CD8+ T cells (**3**), macrophages (**4**), and cancer cells (**5**)], whereas scarcely efficient and selective targeting of splenic T_{reg} in tumor-bearing mice is depicted by crossed small arrows pointing to splenic cells.

subpopulations residing in healthy tissues and tumors; high affinity clones of available ligands against those markers were selected; the *ex vivo* dependence of PEG-SWCNT T_{reg}-targeting efficiency and selectivity on number of antibodies per nanoparticle, incubation time, and dose was investigated; the pharmacokinetic profile of ligand-loaded PEG-SWCNTs and their *in vivo* targeting of intratumor T_{reg} was assessed. Our results showed that PEG-SWCNTs conjugated with ligands against the glucocorticoid-induced TNFR-related receptor (GITR) were preferentially uptaken by T_{reg} residing in the microenvironment of a B16 melanoma while much less efficiency and almost no selectivity was evident in the spleen. This is the first example of intratumor immune cell targeting and we hope it will pave the way to innovative immunotherapies against cancer.

PEG-SWCNTs were fabricated by a noncovalent protocol based on the adsorption of PEG-modified phospholipids onto SWCNT sidewalls and the successive decoration with fluorochromes and targeting ligands.[28,29] We characterized the nanoparticles by elemental analysis, UV−vis spectroscopy, and atomic force microscopy (AFM). The nanoparticles were free from metallic impurities and sterile. As suggested by AFM (Figures 2A and S2) and the sharp peaks in the UV−vis
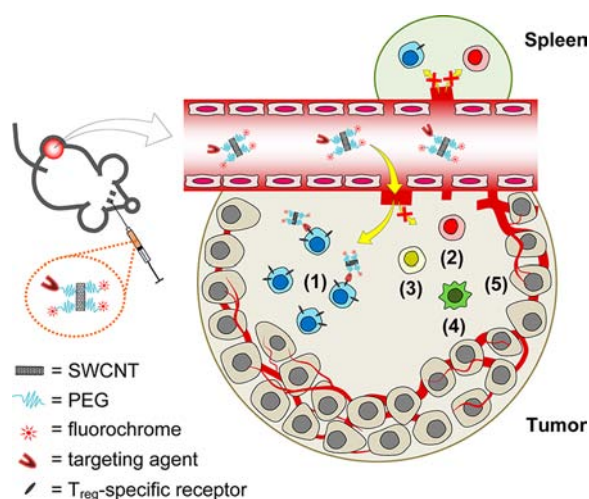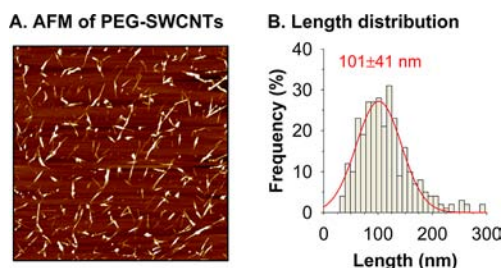

Figure 2. PEG-SWCNTs used for intratumor T_{reg}-specific targeting. A. AFM image of PEG-SWCNTs deposited on mica (scan size 2.5 × 2.5 μm^2). B. PEG-SWCNT length distribution ($n = 300$).

absorption spectrum corresponding to van Hove singularity transitions (data not shown), a stable dispersion of individual nanoparticles was formed under physiological conditions (see Supporting Information). The length of PEG-SWCNTs was measured by AFM (101 ± 41 nm, Figure 2B). We calculated that the density of PEG chains on the PEG-SWCNTs was equal to approximately 0.14 mmol per gram of nanotube material, which corresponds to ∼24 PEG chains per nanotube (see Supporting Information).

In order to achieve T_{reg}-selective delivery of therapeutic cargo (active targeting), we sought markers preferentially expressed on T_{reg}. We assessed the expression of four known T_{reg}-enriched markers, GITR,[30] folate receptor 4 (FR4),[31] CD39,[32] and CD103,[33] and found that GITR and FR4 are enriched in T_{reg} vs T_{eff}. Importantly, all four markers showed increased expression on intratumor vs splenic T_{reg} (Figure S1B), a feature that could be exploited to further increase specificity of delivery to intratumor T_{reg}. GITR showed the highest expression on intratumor T_{reg} and was prioritized for further investigation (Figure S1B).

We tested two commercially available clones of anti-GITR mAbs, DTA-1, and YGITR 765, and found that DTA-1 has higher affinity for GITR than YGITR 765 (Figure S3). Therefore, we selected DTA-1 as the ligand for active nanoparticle targeting. In preliminary experiments we found
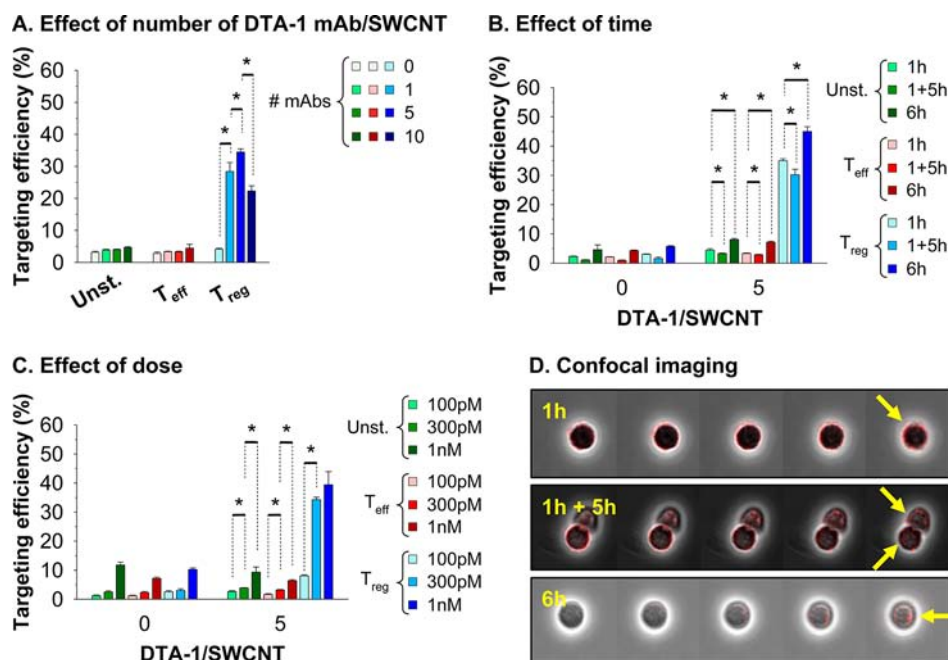
Figure 3. A−C. *Ex vivo* effect of number of ligands per nanotube, incubation time, and dose on PEG-SWCNT-DTA1 T cell-targeting efficiency. A. Total splenocytes from 4- to 8-week-old C57BL/6J GFP-FoxP3 mice were incubated with 300 pM of DyLight650-labeled PEG-SWCNTs loaded with 0, 1, 5, or 10 anti-GITR (clone DTA-1) mAb/SWCNT in PBS for 1 h. Splenocytes treated with PBS alone were used as control. B. Total splenocytes were incubated with 300 pM of DyLight650-labeled PEG-SWCNTs loaded with 0 or 5 anti-GITR (clone DTA-1) mAb/SWCNT in PBS for 1 h, 6 h, or cultured for additional 5 h after 1 h of nanoparticle incubation. C. Total splenocytes were incubated with 100 pM, 300 pM, or 1 nM of DyLight650-labeled PEG-SWCNTs loaded with 0 or 5 anti-GITR (clone DTA-1) mAb/SWCNT in PBS. Next, splenocytes were stained with eFluor 450 anti-CD4 mAb and subjected to FACS analysis. Cells were gated as unstained cells (CD4⁻FoxP3⁻), T_{eff} (CD4⁺FoxP3⁻), and T_{reg} (CD4⁺FoxP3⁺) as in Figure S1A. All experiments were performed in triplicate. Data (mean ± standard deviation) show the frequency of cells with fluorescence higher than the 99.9th percentile of control (PBS-treated) cells as a measure of targeting efficiency. Statistical analysis was performed through the nonparametric Mann−Whitney U analysis (* $0.01 < p \leq 0.05$). D. *Ex vivo* intracellular trafficking of PEG-SWCNTs (confocal microscopy). Confocal images of a sequence of 500-nm-thick slices (from left to right: starting from the upper face to approximately cell center) were taken from representative T_{reg} sorted from total splenocytes from 4- to 8-week-old C57BL/6J GFP-FoxP3 mice incubated with 300 pM of DyLight650-labeled PEG-SWCNTs loaded with 5 anti-GITR (clone DTA-1) mAb/SWCNT in PBS for 1 h, cultured for additional 5 h after 1 h of nanoparticle incubation, or 6 h. Yellow arrows indicate that PEG-SWCNTs were first entrapped into endo/lysosomal compartments (upper panel) translocated to the perinuclear region, and finally released into the cytoplasm and transported into the nucleus of T_{reg} (middle and lower panels).

that after conjugation to PEG-SWCNTs, DTA-1 enabled efficient and selective *in vitro* internalization of the nanoparticles into the cytoplasm (and, although in much lower amounts, into the nucleus) of Jurkat T cells transfected with a GITR expression vector compared to nontransfected cells (Figure S4). Jurkat cells constitutively express very low levels of GITR on their plasma membrane; thus, they represent a good model for preliminary investigations about the targeting efficiency and selectivity of GITR-targeted PEG-SWCNTs. Next, we investigated the effects of number of antibodies per nanotube (mAb/SWCNT), incubation time and dose on the T_{reg}-targeting efficiency (assessed as percentage of PEG-SWCNT⁺ cells in a cell subpopulation), and selectivity (ratio between SWCNT⁺ cells among two cell subpopulations) of PEG-SWCNT-DTA1 *ex vivo*. Total splenocytes from 4- to 8-week-old GFP-FoxP3 knock-in (KI) mice were incubated for 1 h with 300 pM of PEG-SWCNTs carrying 1, 5, or 10 DTA-1/SWCNT.[34] FACS analysis showed that increasing the density of DTA-1/SWCNT from 1 to 5 led to an increase in T_{reg} targeting efficiency and selectivity, whereas increasing the DTA-1 density to 10 DTA-1/SWCNT resulted in overall decreased efficiency and selectivity (Figures 3A and S5A).[35,36] Next, total splenocytes were incubated with 300 pM of PEG-SWCNTs carrying 5 DTA-1/SWCNT for 1 or 6 h, or cultured for additional 5 h after 1 h of nanoparticle incubation. FACS

analysis showed that increasing the incubation time from 1 to 6 h led to a very small increase in T_{reg}-targeting efficiency (Figure 3B) and a decrease in both T_{reg} vs CD4⁻FoxP3⁻ and T_{reg} vs T_{eff} targeting selectivity due to increased nonspecific nanotube uptake (Figure S5B). Cells cultured for additional 5 h after 1 h of nanoparticle incubation showed a minimal decrease in targeting efficiency for all cell subpopulations and no change in targeting selectivity compared to 1 h of incubation (Figures 3B and S5B). These results suggest that cells undergo almost maximal internalization of nanoparticles after short incubation times, and retain the internalized material for a long time even after the nanoparticles are washed away from the media. Finally, we assessed the effect of different concentrations (100, 300, and 1000 pM) of PEG-SWCNTs carrying 5 DTA-1/SWCNT for 1 h. FACS analysis showed that increasing nanoparticle concentration from 100 pM to 300 pM resulted in increased T_{reg}-targeting efficiency (Figure 3C) and both T_{reg} vs CD4⁻FoxP3⁻ cells and T_{reg} vs T_{eff} selectivity (Figure S5C); however, higher nanoparticle concentrations (1 nM) did not result in further increased targeting efficiency or increased selectivity (Figures 3C and S5C).

We investigated the mechanism of T_{reg}-internalization of PEG-SWCNT-DTA1 and found that the nanoparticles were internalized through an energy-dependent mechanism (likely postreceptor engagement endocytosis) (Figure S6). The
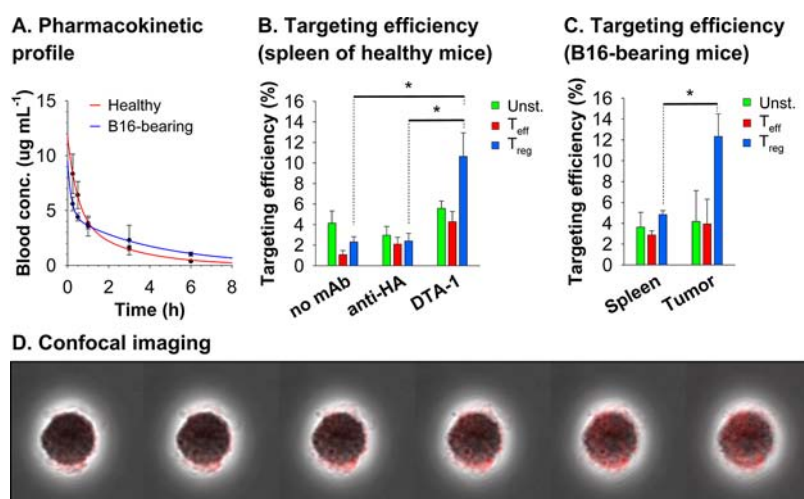
Figure 4. *In vivo* T_{reg} targeting by PEG-SWCNTs. A. Groups of three 4–8-week-old C57BL/6J healthy or B16-bearing littermate mice were given a single injection of 20 μg PEG-SWCNT-DTA1 labeled with 750 nm-emitting fluorochrome in 100 μL of PBS. Blood samples (approximately 100 μL) were collected at different time points and their NIR-emission was measured to calculate the concentration of PEG-SWCNT-DTA1 (μg/mL) in the blood. To calculate the pharmacokinetic parameters of PEG-SWCNT-DTA1 (Table 1), the values of PEG-SWCNT-DTA1 concentration in the blood were fitted to a two-compartment model. B. Groups of three 4–8-week-old C57BL/6J GFP-FoxP3 littermate mice were given a single injection of 5 μg of DyLight650-labeled PEG-SWCNTs loaded with 5 anti-GITR mAb/SWCNT, 5 anti-HA mAb/SWCNT, or ligand-devoid. Splenocytes were collected after 24 h, stained with eFluor 450 anti-CD4 mAb, and subjected to FACS analysis. Cells were gated as unstained cells ($CD4^-FoxP3^-$), T_{eff} ($CD4^+FoxP3^-$), and T_{reg} ($CD4^+FoxP3^+$) as in Figure S1A. Experiments were performed in triplicate. Data (mean ± standard deviation) show the frequency of cells with fluorescence higher than the 99th percentile of cells from control (PBS-treated) mice as a measure of targeting efficiency. Statistical analysis was performed through the nonparametric Mann–Whitney U analysis (* $0.01 < p \leq 0.05$). C. 4–8-week-old C57BL/6J GFP-FoxP3 littermate mice carrying palpable tumors of 6–8 mm in diameter were given a single injection of 5 μg of DyLight650-labeled PEG-SWCNTs loaded with 5 anti-GITR mAb/SWCNT. Splenocytes and B16 tumor cells were collected after 24 h, stained with eFluor 450 anti-CD4 mAb, and subjected to FACS analysis. Cells were gated as unstained cells ($CD4^-FoxP3^-$), T_{eff} ($CD4^+FoxP3^-$), and T_{reg} ($CD4^+FoxP3^+$) as in Figure S1A. Experiments were performed in triplicate. Data (mean ± standard deviation) show the frequency of cells with fluorescence higher than the 99th percentile of cells from control (PBS-treated) mice as a measure of targeting efficiency. Statistical analysis was performed through nonparametric Mann–Whitney U analysis (* $0.01 < p \leq 0.05$). D. Confocal images of sequences of 500-nm-thick slices (from left to right: starting from the upper face to approximately cell center) were taken from representative T_{reg} cells sorted from splenocytes isolated from treated healthy mice. The scattered fluorescence in the last slices (approximately cell center) suggested that PEG-SWCNTs reached the cytoplasm and nucleus of T_{reg} *in vivo*.

nanoparticles' intracellular trafficking was also investigated. T_{reg} were sorted from total splenocytes incubated with PEG-SWCNT-DTA1 for 1 h, 6 h, or cultured for additional 5 h after 1 h incubation and visualized by confocal fluorescence microscopy. Confocal images of T_{reg} central planes showed punctate structures in the proximity of the plasma membrane in cells incubated for 1 h; these structures moved into the cytoplasm or gave way to a diffuse nuclear fluorescence after 5 h of additional incubation in nanoparticle-free media. A diffuse nuclear fluorescence of T_{reg} was also observed in cells incubated for 6 h in nanoparticle-containing media (Figures 3D and S7). Taken together these results suggested that PEG-SWCNT-DTA1 are internalized by T_{reg} through GITR-mediated endocytosis and entrapped into endosomes, which then fuse with lysosomes. Next, the nanoparticles are released into the cytoplasm and finally transported into the cell nucleus (see Supporting Information).[37]

Using a similar approach, we tested the *ex vivo* T_{reg} targeting efficiency and selectivity of PEG-SWCNTs conjugated to anti-FR4, anti-CD103, and anti-CD39 mAbs (Figure S8). These investigations showed that the maxima of T_{reg} targeting efficiency and selectivity were proportional to the levels of marker expression in the following order: GITR > FR4 > CD39 (Figure S9). We also assessed the targeting efficiency and selectivity of PEG-SWCNTs targeted to another very important intratumor T cell subpopulation (CD8$^+$ T cells) by using anti-CD8a mAbs.[38] PEG-SWCNTs showed the best combination of

CD8$^+$ T cell-targeting efficiency and selectivity when loaded with less than 5 anti-CD8a mAb/SWCNT (Supporting Information and Figure S8D).

Next, we investigated the *in vivo* targeting efficiency and selectivity of PEG-SWCNT-DTA1. First we assessed the pharmacokinetic profile of the nanoparticles to confirm that appropriate serum nanoparticle concentration could be achieved and maintained for sufficient time after parenteral injection. Groups of three C57BL/6J littermate mice received a single retro-orbital injection of 20 μg of PEG-SWCNTs carrying 5 DTA-1/SWCNT and labeled with NIR-emitting fluorochromes. NIR emissions of blood samples collected at different time points were measured, the values of PEG-SWCNT-DTA1 concentration in the blood calculated and fitted to a two-compartment model ($R = 1$) (Figure 4A), and the pharmacokinetic parameters of PEG-SWCNT-DTA1 calculated (Table 1 and Supporting Information).[39] Next, groups of three GFP-FoxP3 littermate mice received single retro-orbital injection of different amounts of PEG-SWCNTs carrying 5 DTA-1/SWCNT and were sacrificed 24 h after administration. Splenocytes were isolated and subjected to FACS analysis. In line with our previous *ex vivo* findings that use of higher concentrations of nanoparticles does not automatically translate into better targeting efficiency and selectivity (Figures 3C and S5C) we found that the best uptake efficiency and selectivity occurred in mice treated with relatively low doses (5 μg) of targeted nanoparticles (Table S1 and

Table 1. Pharmacokinetic Parameters of PEG-SWCNT-DTA1[a]

	$T_{0.5\alpha}$ [h]	$T_{0.5\beta}$ [h]	AUC_∞ [h μg mL^{-1}]	V_c [mL]	V_{ss} [mL]	V_β [mL]	C_β [mL h^{-1}]
Healthy mice	0.4	1.9	15.2	1.7	2.8	3.5	1.3
B16-bearing mice	0.1	2.9	16	2.1	4	5.2	1.3

[a]Groups of three C57BL/6J healthy or B16-bearing littermate mice were retro-orbitally given a single injection of 20 μg of PEG-SWCNT-DTA1 labeled with a 750-nm-emitting fluorochrome in 100 μL of PBS. Blood samples were collected at different time points, and the near infrared (NIR)-emission of each sample was measured and used to obtain the pharmacokinetic parameters of PEG-SWCNT-DTA1 (see Supporting Information). $T_{0.5\alpha}$ = distribution half-life; $T_{0.5\beta}$ = elimination half-life; AUC_∞ = area under the concentration curve; V_c = volume of distribution of the central compartment; V_{ss} = volume of distribution in steady state; V_β = volume of distribution in β-phase; C_β = clearance.

Figure 4B). A very low nonspecific internalization into T_{reg} was observed when mice were injected with 5 μg of PEG-SWCNTs loaded with 5 control (anti-HA) mAbs or no mAb (Figure 4B). In order to ensure that the nanoparticles underwent internalization *in vivo*, we assessed their localization by confocal microscopy. T_{reg} were sorted from splenocytes of GFP-FoxP3 littermate mice retro-orbitally injected with 5 μg of PEG-SWCNTs loaded with 5 DTA-1/SWCNT and sacrificed 24 h postadministration. Confocal microscopy revealed that PEG-SWCNT-DTA1 were diffusely localized within the cytosol and nucleus of T_{reg} of treated mice (Figure 4D).[37]

Finally, we validated the hypothesis that ligand-conjugated PEG-SWCNTs undergo intratumor enrichment and enable preferential *in vivo* targeting of intratumor T_{reg}. First we assessed the pharmacokinetic profile of PEG-SWCNT-DTA1 in B16-bearing mice. Groups of three C57BL/6J B16-bearing littermate mice received a single retro-orbital injection of 20 μg of PEG-SWCNTs carrying 5 DTA-1/SWCNT and labeled with NIR-emitting fluorochromes. Blood samples were collected at different time points, their NIR emission recorded, and the blood concentration of PEG-SWCNT-DTA1 as a function of time calculated (Figure 4A). The pharmacokinetic parameters of PEG-SWCNT-DTA1 are reported in Table 1. It is worth noting that PEG-SWCNT-DTA1 exhibited a 4-fold lower distribution half-life and a slightly higher elimination half-life in B16-bearing mice with respect to healthy mice. Differences in the circulation time of spherical nanoparticles in healthy and tumor-bearing mice have been described.[40] This phenomenon could be due to fast nanoparticle extravasation from tumor vessels, which may explain the faster distribution half-life of nanotubes in tumor-bearing mice with respect to healthy mice, and/or differences between the protein corona adsorbed onto nanoparticles circulating in the bloodstream of tumor-bearing mice and that adsorbed onto nanoparticles circulating in the bloodstream of healthy mice.[41] Next, we retro-orbitally injected groups of three GFP-FoxP3 B16-bearing littermate mice with a single 5 μg dose of PEG-SWCNTs carrying 5 DTA-1/SWCNT and sacrificed the animals 24 h postadministration. We found that PEG-SWCNT-DTA1 targeted intratumor T_{reg} with more than 3-fold higher efficiency with respect to splenic T_{reg}, whereas the efficiency of T_{eff}-targeting was similar for both tumor tissue and spleen (Figure 4C). Due to a pathologic increase in the T_{reg}:T_{eff} ratio (Figure S1A) in the tumor microenvironment, this translated into an approximately 10-fold higher T_{reg}:T_{eff} targeting selectivity in the tumor tissue vs the spleen. Interestingly, although tumor-bearing mice displayed a nearly doubled number of splenic T_{reg} compared to healthy animals, splenic T_{reg} were targeted with much less efficiency in tumor-bearing vs healthy mice. Thus, the splenic T_{reg}:T_{eff} targeting selectivity of PEG-SWCNT-DTA1 was comparable between healthy and tumor-bearing mice.

In summary, we investigated the ability of T_{reg}-specific receptors to drive internalization of PEG-SWCNTs into T_{reg} *ex vivo* and *in vivo*. We focused our attention on the glucocorticoid-induced TNFR-related receptor (GITR), as it showed higher overexpression on intratumor vs splenic T_{reg} compared to other reportedly T_{reg}-specific markers (FR4, CD103, and CD39) (Figure S1B). Our *ex vivo* investigations using splenocytes collected from healthy mice showed that the targeting efficiency and selectivity of PEG-SWCNTs depend on number of ligands per nanotube, incubation time, dose, and targeted surface marker. PEG-SWCNTs loaded with GITR ligands (anti-GITR mAbs, clone DTA-1) were internalized by T_{reg} through receptor-mediated endocytosis and transported into the cytoplasm and nucleus *ex vivo* and *in vivo*. Importantly, injection of PEG-SWCNT-DTA1 in animals carrying tumors enabled very good targeting of T_{reg} residing in the tumor microenvironment, while much less efficiency and almost no selectivity was evident in the spleen. The mechanism of this interesting phenomenon remains to be elucidated; however, we speculate that preferential penetration of nanoparticles into the tumor microenvironment compared to other tissues (i.e., spleen) was a consequence of EPR effect. The naturally increased intratumor T_{reg} vs T_{eff} ratio and the use of markers that are enriched in intratumor vs peripheral T_{reg} (i.e., GITR) helped increase the efficiency and selectivity of intratumor T_{reg} targeting.

This investigation is the first example of selective intratumor targeting of T_{reg}, and we hope it will pave the way to novel oncologic immunotherapies based on T_{reg}-selective functional manipulation. Further optimization of the technology and improved understanding of the physiological variables affecting its success are needed in order to increase translatability. This includes a deeper knowledge of the molecular pathways driving the functions of intratumor T_{reg} and of the phenotype/surface markers of human T_{reg} (i.e., pro- vs antitumor) and the development of new ligands for intratumor T_{reg} and other intratumor immune cell populations.[6,7]

ASSOCIATED CONTENT

Supporting Information

Materials and methods; characterization of PEG-SWCNTs; investigation of GITR-affinity for DTA-1 and YGITR 765 clones; targeting of GITR$^+$ Jurkat cells by PEG-SWCNTs; *ex vivo* T_{reg} and CD8$^+$ T cell targeting by PEG-SWCNTs; calculation of the PEG-SWCNTs' pharmacokinetic parameters. This material is available free of charge via the Internet at http://pubs.acs.org.

AUTHOR INFORMATION

Corresponding Author

*Nunzio Bottini: Phone (858) 752-6815; Fax (858) 752-6985; E-mail: nunzio@liai.org. Massimo Bottini: Phone 858-646-3100 x3063; Fax 858-713-9925; E-mail: mbottini@sanfordburnham.org.

■ **REFERENCES**

(1) Whiteside, T. L. (2012) What are regulatory T Cells (Treg) regulating in cancer and why? *Semin. Cancer. Biol.* 22, 327−334.

(2) Mougiakakos, D., Choudhury, A., Lladser, A., Kiessling, R., and Johansson, C. C. (2010) Regulatory T cells in cancer. *Adv. Cancer Res.* 107, 57−117.

(3) Ghiringhelli, F., Puig, P. E., Roux, S., Parcellier, A., Schmitt, E., Solary, E., Kroemer, G., Martin, F., Chauffert, B., and Zitvogel, L. (2005) Tumor cells convert immature myeloid dendritic cells into TGF-beta-secreting cells inducing CD4+CD25+ regulatory T cell proliferation. *J. Exp. Med.* 202, 919−929.

(4) Zhou, G., and Levitsky, H. I. (2007) Natural regulatory T cells and de novo-induced regulatory T cells contribute independently to tumor-specific tolerance. *J. Immunol.* 178, 2155−2162.

(5) Valzasina, B., Piconese, S., Guiducci, C., and Colombo, M. P. (2006) Tumor-induced expansion of regulatory T cells by conversion of CD4+CD25- lymphocytes is thymus and proliferation independent. *Cancer Res.* 66, 4488.

(6) Salama, P., Phillips, M., Grieu, F., Morris, M., Zeps, N., Joseph, D., Platell, C., and Iacopetta, B. (2009) Tumor-infiltrating FOXP3+ T regulatory cells show strong prognostic significance in colorectal cancer. *J. Clin. Oncol.* 27, 186−192.

(7) Frey, D. M., Droeser, R. A., Viehl, C. T., Zlobec, I., Lugli, A., Zingg, U., Oertli, D., Kettelhack, C., Terracciano, L., and Tornillo, L. (2010) High frequency of tumor-infiltrating FOXP3(+) regulatory T cells predicts improved survival in mismatch repair-proficient colorectal cancer patients. *Int. J. Cancer* 126, 2635−2643.

(8) Colombo, M. P., and Piconese, S. (2007) Regulatory-T-cell inhibition versus depletion: the right choice in cancer immunotherapy. *Nat. Rev. Cancer* 7, 880−887.

(9) Vanneman, M., and Dranoff, G. (2012) Combining immunotherapy and targeted therapies in cancer treatment. *Nat. Rev. Cancer* 12, 237−251.

(10) Peer, D., Karp, J. M., Hong, S., Farokhzad, O. C., Margalit, R., and Langer, R. (2007) Nanocarriers as an emerging platform for cancer therapy. *Nat. Nanotechnol.* 2, 751−760.

(11) Cheng, Z., Al Zaki, A., Hui, J. Z., Muzykantov, V. R., and Tsourkas, A. (2012) Multifunctional nanoparticles: cost versus benefit of adding targeting and imaging capabilities. *Science* 338, 903−910.

(12) Singh, R., and Nalwa, H. S. (2011) Medical applications of nanoparticles in biological imaging, cell labeling, antimicrobial agents, and anticancer nanodrugs. *J. Biomed. Nanotechnol.* 7, 489−503.

(13) *Lecture Notes in Nanoscale Science and Technology. Vol. 4: Nanoparticles and nanodevices in Biological Applications* (Bellucci, S., Ed.) (2009) Springer-Verlag, Berlin.

(14) Bottini, M., Rosato, N., and Bottini, N. (2011) PEG-modified carbon nanotubes in biomedicine: current status and challenges ahead. *Biomacromolecules* 12, 3381−3393.

(15) O'Connell, M. J., Bachilo, S. M., Huffman, C. B., Moore, V. C., Strano, M. S., Haroz, E. H., Rialon, K. L., Boul, P. J., Noon, W. H., Kittrell, C., Ma, J., Hauge, R. H., Weisman, R. B., and Smalley, R. E. (2002) Band gap fluorescence from individual single-walled carbon nanotubes. *Science* 297, 593−596.

(16) Welsher, K., Liu, Z., Sherlock, S. P., Robinson, J. T., Chen, Z., Daranciang, D., and Dai, H. (2009) A route to brightly fluorescent carbon nanotubes for near-infrared imaging in mice. *Nat. Nanotechnol.* 4, 773−780.

(17) Liu, Z., Li, X., Tabakman, S. M., Jiang, K., Fan, S., and Dai, H. (2008) Multiplexed multicolor raman imaging of live cells with isotopically modified single walled carbon nanotubes. *J. Am. Chem. Soc.* 130, 13540−13541.

(18) Liu, Z., Davis, C., Cai, W., He, L., Chen, X., and Dai, H. (2008) Circulation and long-term fate of functionalized, biocompatible single-walled carbon nanotubes in mice probed by raman spectroscopy. *Proc. Natl. Acad. Sci. U.S.A.* 105, 1410−1415.

(19) Prencipe, G., Tabakman, S. M., Welsher, K., Liu, Z., Goodwin, A. P., Zhang, L., Henry, J., and Dai, H. (2009) PEG branched polymer for functionalization of nanomaterials with ultralong blood circulation. *J. Am. Chem. Soc.* 131, 4783−4787.

(20) Schipper, M. L., Nakayama-Ratchford, N., Davis, C. R., Kam, N. W., Chu, P., Liu, Z., Sun, X., Dai, H., and Gambhir, S. S. (2008) A pilot toxicology study of single-walled carbon nanotubes in a small sample of mice. *Nat. Nanotechnol.* 3, 216−221.

(21) Fabbro, C., Ali-Boucetta, H., Da Ros, T., Kostarelos, K., Bianco, A., and Prato, M. (2012) Targeting carbon nanotubes against cancer. *Chem. Commun. (Camb.)* 48, 3911−3926.

(22) Robinson, J. T., Hong, G., Liang, Y., Zhang, B., Yaghi, O. K., and Dai, H. (2012) In vivo fluorescence imaging in the second near-infrared window with long circulating carbon nanotubes capable of ultrahigh tumor uptake. *J. Am. Chem. Soc.* 134, 10664−10669.

(23) Smith, B. R., Kempen, P., Bouley, D., Xu, A., Liu, Z., Melosh, N., Dai, H., Sinclair, R., and Gambhir, S. S. (2012) Shape matters: intravital microscopy reveals surprising geometrical dependence for nanoparticles in tumor models of extravasation. *Nano Lett.* 12, 3369−3377.

(24) Liu, Z., Chen, K., Davis, C., Sherlock, S., Cao, Q., Chen, X., and Dai, H. (2008) Drug delivery with carbon nanotubes for in vivo cancer treatment. *Cancer Res.* 68, 6652−6660.

(25) Chen, J., Chen, S., Zhao, X., Kuznetsova, L. V., Wong, S. S., and Ojima, I. (2008) Functionalized single-walled carbon nanotubes as rationally designed vehicles for tumor-targeted drug delivery. *J. Am. Chem. Soc.* 130, 16778−16785.

(26) Villa, C. H., McDevitt, M. R., Escorcia, F. E., Rey, D. A., Bergkvist, M., Batt, C. A., and Scheinberg, D. A. (2008) Synthesis and biodistribution of oligonucleotide-functionalized, tumor-targetable carbon nanotubes. *Nano Lett.* 8, 4221−4228.

(27) McDevitt, M. R., Chattopadhyay, D., Kappel, B. J., Jaggi, J. S., Schiffman, S. R., Antczak, C., Njardarson, J. T., Brentjens, R., and Scheinberg, D. A. (2007) Tumor targeting with antibody-functionalized, radiolabeled carbon nanotubes. *J. Nucl. Med.* 48, 1180−1189.

(28) Cato, M. H., D'Annibale, F., Mills, D. M., Cerignoli, F., Dawson, M. I., Bergamaschi, E., Bottini, N., Magrini, A., Bergamaschi, A., Rosato, N., Rickert, R. C., Mustelin, T., and Bottini, M. (2008) Cell-type specific and cytoplasmic targeting of PEGylated carbon nanotube-based nanoassemblies. *J. Nanosci. Nanotechnol.* 8, 2259−2269.

(29) Delogu, L. G., Stanford, S. M., Santelli, E., Magrini, A., Bergamaschi, A., Motamedchaboki, K., Rosato, N., Mustelin, T., Bottini, N., and Bottini, M. (2010) Carbon nanotube-based nanocarriers: the importance of keeping it clean. *J. Nanosci. Nanotechnol.* 10, 5293−5301.

(30) Shimizu, J., Yamazaki, S., Takahashi, T., Ishida, Y., and Sakaguchi, S. (2002) Stimulation of CD25(+)CD4(+) regulatory T cells through GITR breaks immunological self-tolerance. *Nat. Immunol.* 3, 135−142.

(31) Yamaguchi, T., Hirota, K., Nagahama, K., Ohkawa, K., Takahashi, T., Nomura, T., and Sakaguchi, S. (2007) Control of immune responses by antigen-specific regulatory T cells Expressing the folate receptor. *Immunity* 27, 145−159.

(32) Deaglio, S., Dwyer, K. M., Gao, W., Friedman, D., Usheva, A., Erat, A., Chen, J. F., Enjyoji, K., Linden, J., Oukka, M., Kuchroo, V. K., Strom, T. B., and Robson, S. C. (2007) Adenosine generation

catalyzed by CD39 and CD73 expressed on regulatory T cells mediates immune suppression. *J. Exp. Med. 204*, 1257−1265.

(33) Anz, D., Mueller, W., Golic, M., Kunz, W. G., Rapp, M., Koelzer, V. H., Ellermeier, J., Ellwart, J. W., Schnurr, M., Bourquin, C., and Endres, S. (2011) CD103 is a hallmark of tumor-infiltrating regulatory T cells. *Int. J. Cancer 129*, 2417−2426.

(34) Fontenot, J. D., Rasmussen, J. P., Williams, L. M., Dooley, J. L., Farr, A. G., and Rudensky, A. Y. (2005) Regulatory T cell lineage specification by the forkhead transcription factor FoxP3. *Immunity 22*, 329−341.

(35) Elias, D. R., Poloukhtine, A., Popik, V., and Tsourkas, A. Effect of ligand density, receptor density, and nanoparticle size on cell targeting. *Nanomedicine* 2012.

(36) Jiang, W., Kim, B. Y., Rutka, J. T., and Chan, W. C. (2008) Nanoparticle-mediated cellular response is size-dependent. *Nat. Nanotechnol. 3*, 145−150.

(37) Mu, Q., Broughton, D. L., and Yan, B. (2009) Endosomal leakage and nuclear translocation of multiwalled carbon nanotubes: developing a model for cell uptake. *Nano Lett. 9*, 4370−4375.

(38) Ercolini, A. M., Ladle, B. H., Manning, E. A., Pfannenstiel, L. W., Armstrong, T. D., Machiels, J. P., Bieler, J. G., Emens, L. A., Reilly, R. T., and Jaffee, E. M. (2005) Recruitment of latent pools of high-avidity CD8(+) T cells to the antitumor immune response. *J. Exp. Med. 201*, 1591−1602.

(39) Gerlowski, L. E., and Jain, R. K. (1983) Physiologically based pharmacokinetic modeling: principles and applications. *J. Pharm. Sci. 72*, 1103−1127.

(40) Ohno, K., Akashi, T., Tsujii, Y., Yamamoto, M., and Tabata, Y. (2012) Blood clearance and biodistribution of polymer brush-afforded silica particles prepared by surface-initiated living radical polymerization. *Biomacromolecules 13*, 927−936.

(41) Sacchetti, C., Motamedchaboki, K., Magrini, A., Palmieri, G., Mattei, M., Bernardini, S., Rosato, N., Bottini, N., and Bottini, M. (2013) Surface polyethylene glycol conformation influences the protein corona of polyethylene glycol-modified single-walled carbon nanotubes: potential implications on biological performance. *ACS Nano 7*, 1974−1989.

(42) Al-Jamal, K. T., Nunes, A., Methven, L., Ali-Boucetta, H., Li, S., Toma, F. M., Herrero, M. A., Al-Jamal, W. T., ten Eikelder, H. M., Foster, J., Mather, S., Prato, M., Bianco, A., and Kostarelos, K. (2012) Degree of chemical functionalization of carbon nanotubes determines tissue distribution and excretion profile. *Angew. Chem., Int. Ed. Engl. 51*, 6389−6393.